Journal of Power Sources 245 (2014) 841–845

Contents lists available at SciVerse ScienceDirect

Journal of Power Sources

journal homepage: www.elsevier.com/locate/jpowsour

Short communication

A novel nitrogen-containing electrocatalyst for oxygen reduction reaction from blood protein pyrolysis

Chao-Zhong Guo [a,*], Chang-Guo Chen [a,*], Zhong-Li Luo [b]

[a] College of Chemistry and Chemical Engineering, Chongqing University, Chongqing 400044, China
[b] College of Basic Medical Sciences, Molecular Medicine and Cancer Research Center, Chongqing Medical University, Chongqing 400046, China

HIGHLIGHTS

- A novel N-containing electrocatalyst for ORR was fabricated by using pyrolysis of blood protein.
- Addition of carbon support into carbonization process may produce better catalytic activity.
- High-temperature pyrolysis process can transfer the pyridinic-N to pyrrolic-N significantly.
- The content of pyrrolic-N group plays an important role in improvement of the ORR catalytic activity.

ARTICLE INFO

Article history:
Received 19 April 2013
Received in revised form
5 July 2013
Accepted 7 July 2013
Available online 16 July 2013

Keywords:
Oxygen reduction
Electrocatalyst
Blood protein
Pyrolysis

ABSTRACT

We report a new strategy to design carbon-based electrocatalysts containing nitrogen through the co-pyrolysis of blood protein and carbon black support. The results show that the nitrogen in electrocatalysts is primarily in the form of pyridinic- and pyrrolic-type nitrogen species. High-temperature pyrolysis processes can transfer a significant amount of pyridinic-N to pyrrolic-N. The electrocatalyst containing a higher amount of the pyrrolic-N configuration exhibits better electrocatalytic activity towards oxygen reduction reaction in terms of onset potential, half-wave potential, and limited current density. It is suggested that the pyrrolic-N configuration may be the electrocatalytically active site and may be responsible for the enhanced ORR performance in alkaline media. The carbon black support also plays an important role in the pyrolysis process, improving the ORR catalytic activity.

1. Introduction

The oxygen reduction reaction (ORR) at the cathode plays a key role in metal–air batteries [1] and fuel cells [2]. Carbon-supported platinum particles are the most effective catalyst for the ORR [3], but sluggish oxygen reduction, high cost, and low abundance limit the commercialization of these technologies. Many research efforts have been done on the reduction of Pt loading and exploration of novel non-precious catalysts to reduce fuel cell cost. It is interesting that heat-treated carbon materials have received enormous attention as non-precious electrode materials for ORR, especially for N-doped carbon nanotubes and N-doped graphene [4–7]. Additional N-containing materials were fabricated by several bioproteins, such as collagen [8] and hemoglobin [9,10]. Quite recently, several groups have reported the preparation and oxygen reduction electrocatalytic behavior of N-containing electrocatalysts using hemin biomaterial as an effective precursor or N-enriched amino acids as nitrogen sources [11–15]. These works mainly focus on the use of natural porphyrinatoiron complexes contained inside hemin or the selection of nitrogen sources to form the catalytic sites.

Many heat-treated materials have reasonably good electrocatalytic activity towards ORR, but their stability is still far below the requirements for the practical application of new energy. The exhibited catalytic properties may be substantially attributed to the presence of C–N active sites in the carbon structure [4,16–19]. However, the detailed C–N bonding configuration responsible for the ORR catalytic activity of N-containing carbons remains elusive. Additionally, to create N-containing electrocatalysts, in addition to the requirement of complex procedures and expensive equipment, the precursors also need to be handled carefully because of their toxic and corrosive nature [5]. Therefore, the development of a

* Corresponding authors. Tel./fax: +86 023 65111357.
E-mail addresses: guochaozhong1987@163.com (C.-Z. Guo), cgchen@cqu.edu.cn (C.-G. Chen).

0378-7753/$ – see front matter © 2013 Elsevier B.V. All rights reserved.
http://dx.doi.org/10.1016/j.jpowsour.2013.07.037

simple and effective method for fabricating electrocatalysts to replace the commercial Pt-based catalysts has remained a challenge.

Blood protein (BP) from animals can be obtained from the meat industry, and it includes an abundance of hemoprotein and various amino acids. These substances can successfully produce active electrocatalysts for ORR in acidic and alkaline environments. BP material could be a potential precursor for preparing highly active electrocatalysts for ORR, as supported by our previous reports [20]. To overcome the current obstacles, in this work, we develop a new approach to synthesize a novel N-containing electrocatalyst (BP350C1000) BP material with high ORR catalytic activity and stability through the use of high-temperature pyrolysis. Our results indicate that BP350C1000 with higher percentage of pyrrolic-N improves ORR activity substantially, suggesting that pyrrolic-N plays an active role in ORR electrocatalysis.

2. Experiments

2.1. Materials

Porcine BP was supplied by the Food Testing Center of Chongqing Bureau of Quality and Technology Supervision, China. Carbon black (Vulcan XC-72R) was purchased from Cabot® and pretreated in a solution containing 10% HNO_3 and 30% H_2O_2 at 80 °C for 12 h.

2.2. Catalyst preparation

First, 0.5 g of BP was decomposed in flowing N_2 at 350 °C for 5 h. The yielded pyropolymer as a precursor was mixed with the pretreated carbon black support (mass ratio of 1:1) by ball milling. The obtained substance was further treated in flowing N_2 at 1000 °C for 2 h. The produced sample is hereafter called BP350C1000. As a control, the direct high-temperature pyrolysis of BP at 1000 °C for 2 h was used for the fabrication of BP1000. In addition, BP3501000 was obtained by continuous heat-treatment of BP at 350 °C for 5 h and 1000 °C for 2 h without the addition of carbon black.

2.3. Characterization

X-ray diffraction (XRD) analysis was performed using a Shimadzu XRD-6000 X-ray diffractometer (Japan) with Cu $K\alpha_1$ radiation ($\lambda = 1.54178$ Å) at 4° min^{-1}. X-ray photoelectron spectroscopy (XPS) analysis was performed using a VG Scientific ESCALAB 220 iXL spectrometer with an Al $K\alpha$ ($hv = 1486.69$ eV) X-ray source. The specific surface area and pore structure were examined by nitrogen adsorption/desorption analysis. The surface morphology was studied using a Seiko SPA400 atomic force microscope (AFM, Japan).

2.4. Electrochemical measurements

Electrochemical experiments were conducted on a CHI 600A electrochemical workstation (CH instruments, USA). A platinum wire and a Hg/HgO/1 mol l^{-1} KOH electrode were used as the counter and reference electrodes, respectively. A rotation disk electrode (RDE) with a glassy carbon (GC) electrode (5-mm diameter, LKXZ-1, Tianjing Lanlike Electrochemical Instruments, China) was used as working electrode. The modified-GC working electrode was fabricated by coating it with catalyst ink. Typically, 10 μl of catalyst ink, well-dispersed by 0.5 wt.% Nafion/isopropanol solution, was dropped onto the GC disk surface and then dried at room temperature. The mass loading of all samples is equal to ca. 500 μg cm^{-2}. All of the electrode potentials in this study are quoted *versus* a reversible hydrogen electrode (RHE). All RDE experiments for ORR were performed over the potential range of 1.15 to 0.15 V at a scan rate of 5 mV s^{-1} in O_2-saturated 0.1 mol l^{-1} KOH solution. The onset potentials (the potential at which a current density of −50 μA cm^{-2} is recorded) were taken from the ORR polarization curves. The stability of BP350C1000 electrocatalyst was evaluated using an accelerated aging test (AAT). The AAT uses 5000 continuous potential cycles performed by scanning between 0.15 and 1.15 V at a scan rate of 50 mV s^{-1} in 0.1 mol l^{-1} KOH solution purged with N_2. The ORR performance after AAT was further assessed using the same standard three-electrode cell as described above.

3. Results and discussion

3.1. Catalyst characterization

In Fig. 1(a), the XRD patterns of three N-containing electrocatalysts show similar phase compositions. The only other peaks observed are two amorphous-carbon peaks, centered at 2θ values of ≈24° and ≈44°, which are ascribed to the graphitic planes (002) and (101), respectively [20]. The broad peak at 24° reveals the domination of the disordered carbon phase in electrocatalysts, while the weak broad peak at 44° suggests the existence of graphitic layers with smaller sizes and lower three-dimensional order [21]. In contrast, the precursor does not exhibit these highly desirable characteristics but does feature a weak amorphous-carbon peak at ≈21°, which may be due to the unfinished carbonization of the BP350 pyropolymer. High-temperature pyrolysis of the precursor can enrich the activated-carbon sources and increase the degree of graphitization. Furthermore, in the presence of the carbon black support, the 2θ values for the two diffraction peaks in the three electrocatalysts change slightly and increase in width, which can be attributed to the formation of C—N bonding groups into graphitic layers and lower degrees of graphitization.

Fig. 1(b) shows the XPS analysis of the C—N binding configuration and corresponding distribution in all carbonized materials. The fitting data are summarized in Table 1. The presence of nitrogen atoms in the carbon structure is confirmed, producing three main C—N binding configurations: pyridinic-, pyrrolic-, and graphitic-type nitrogen species. The carbonization process of BP mainly results in the pyridinic-N and pyrrolic-N configurations, which is supported by previous reports [6,17,19,22]. An interesting finding is that the pyridinic-N and graphitic-N peaks gradually approach the pyrrolic-N peak as the binding energy changes (≈0.8 eV) from BP1000 to BP350C1000, demonstrating a trend of effectively producing a higher content of pyrrolic-N species inside BP350C1000. High-temperature pyrolysis has led to an obvious increase in the pyrrolic-N percentage from 50.0% for the BP350 precursor to 60.2% for BP350C1000, while the percentage of pyridinic-N decreases significantly. Similar results are obtained for the other catalysts (BP1000 and BP3501000). This finding shows that the transformation of pyridinic-N to pyrrolic-N occurs with high-temperature carbonization.

Based on the N_2 adsorption/desorption isotherms shown in Fig. 1(c), BP350C1000 exhibits a type II isotherm curve, which usually stems from nonporous particles or particles with pores larger than micropores [23]. An overlap of the N_2 adsorption and desorption curves can be clearly observed in the low-relative-pressure range ($P/P_0 \leq 0.7$) of this isotherm curve, while a hysteresis loop exists in the high-relative-pressure range for dense N-modified carbons. This finding indicates the presence of inkbottle-type pores [24], but these pores are dead ends and produce a dense morphology. These results show that some porous particles in the PB350C1000 sample are partially filled by further heating of the BP350 precursor. Moreover, the adsorption average pore size and specific surface area (4 V/A by BET) of BP350C1000 are 11 nm and

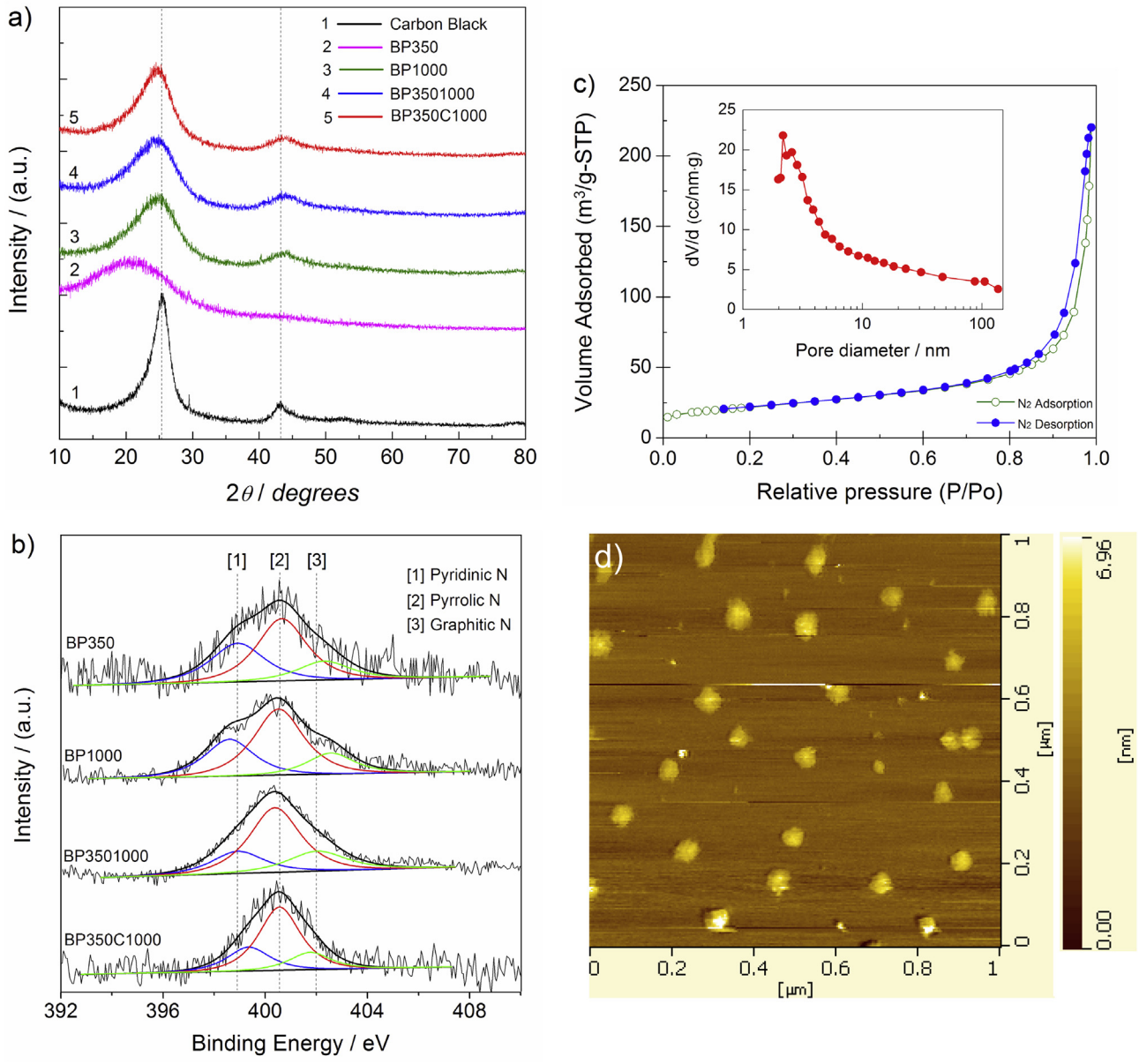

Fig. 1. (a) XRD patterns of carbon black, BP350 precursor, and three electrocatalysts. (b) XPS spectra for the N1s region of the BP350 precursor and three electrocatalysts. (c) N_2 adsorption/desorption isotherms of BP350C1000 and BJH pore-size distribution (inset). (d) AFM image of BP350C1000.

73 $m^2\ g^{-1}$, respectively, which are less than those of the carbon support [25]. The nano-particles are ≈50 nm in size (Fig. 1(d)), which is also larger than the particles of the carbon support (30 nm). The carbon support has been covered and modified with thermally decomposed products, including amino acid residues and fragments of natural metalloporphyrins inside the BP350 precursor, as confirmed by XPS analysis.

Table 1
XPS data: N1s binding energies and relative contents of PB350 precursor and three electrocatalysts. Data are obtained from Fig. 1(b).

Sample	Pyridinic-N		Pyrrolic-N		Graphitic-N	
	B.E./eV	at.%	B.E./eV	at.%	B.E./eV	at.%
BP350	398.9	33.8	400.7	50.0	402.3	16.2
BP1000	398.6	29.4	400.5	54.3	402.6	16.3
BP3501000	398.9	20.6	400.4	58.7	402.0	20.7
BP350C1000	399.4	23.3	400.6	60.2	401.8	16.5

3.2. Electrochemical catalytic activity

The electrocatalytic activity of BP1000, BP3501000, and BP350C1000 for ORR in 0.1 mol l^{-1} KOH solution is shown in Fig. 2(a). Large differences between the ORR activity plots are distinctly visible. All catalytic activity data are summarized in Table 2. BP3501000 has better catalytic activity than BP1000 because the carbon matrix and the active sites are changed by the two-step carbonization [10]. This finding can be mainly ascribed to a large increase in the amount of the pyrrolic-N configuration due to the change in the carbonization process from one to two steps. Notably, BP350C1000 exhibits the most positive onset potential (E_{ORR}) of 0.90 V and half-wave potential (E_{hw}) of 0.78 V, nearly identical to those of the Pt/C catalyst [26]. Based the analysis of such parameters as E_{ORR}, E_{hw}, and the current densities, BP350C1000 exhibits the best ORR performance. This result indicates that using carbon black support as a conductive agent and inserting matrix to form catalytic sites in the carbonization process can greatly

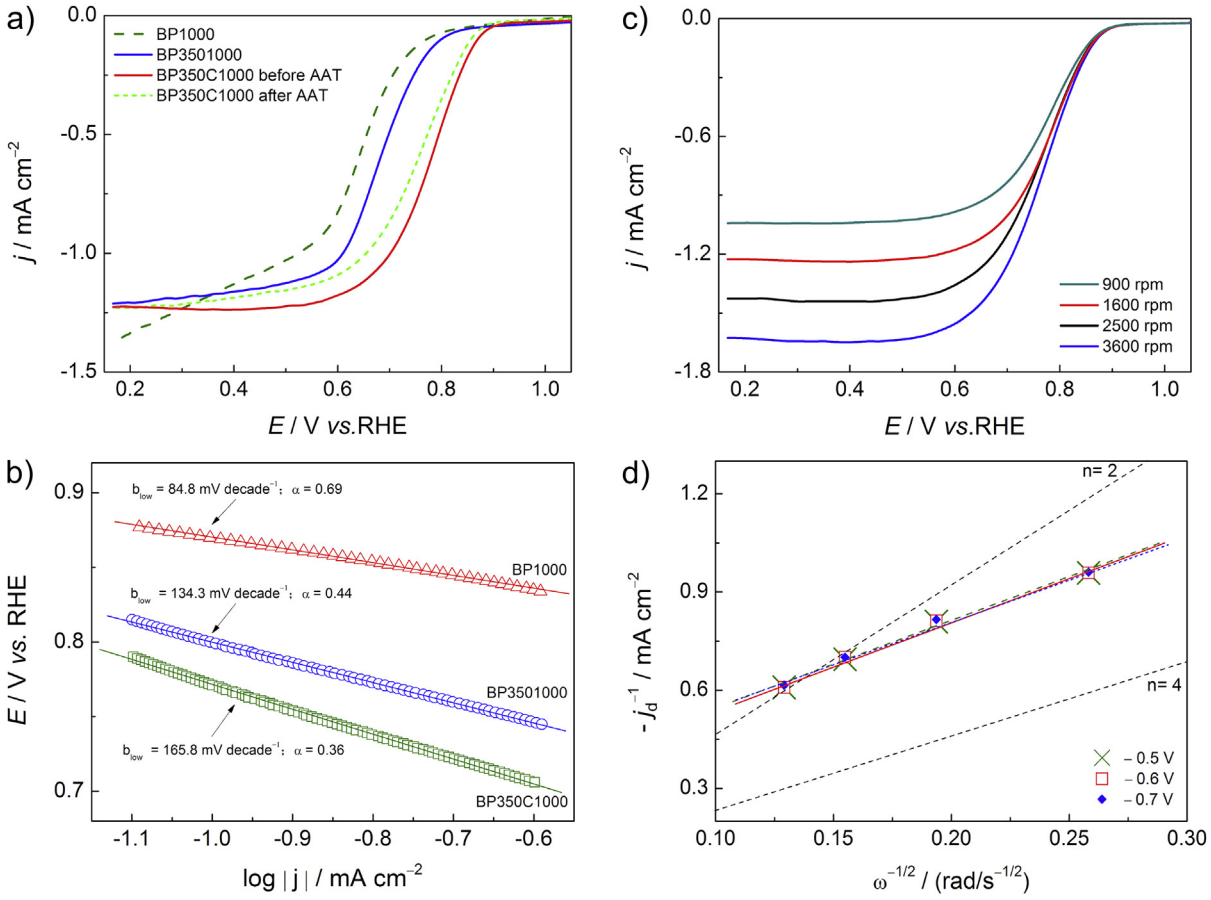

Fig. 2. (a) ORR polarization curves for BP1000, BP3501000, and BP350C1000 before and after AAT at a rotation rate of 1600 rpm. (b) Tafel plots for ORR on BP1000, BP3501000, and BP350C1000. Data are taken from Fig. 2(a). (c) ORR polarization curves for BP350C1000 at various rotation rates. (d) Koutecky–Levich plot of j_d^{-1} vs. $\omega^{-1/2}$ obtained from Fig. 2(c).

enhance its ORR catalytic activity in alkaline media. The difference between BP3501000 and BP350C1000 in the electrocatalytic performance of the ORR is attributed to three aspects: 1) introducing carbon support produces more exposed catalytically active sites [27] and provides a larger space for more active catalytic sites by preventing agglomeration during pyrolysis; 2) the addition of carbon black helps to form new active sites on the modified carbons with other N-containing groups created from further decomposition of the BP350 precursor during high-temperature pyrolysis; and 3) a greater amount of the pyrrolic-N configuration is produced in BP350C1000 than in BP3501000.

The electrocatalytic activity of N-containing carbon-based electrocatalysts is strongly dependent on the nitrogen configuration, which is mainly pyrrolic, pyridinic, or graphitic [28,29]. The electron-withdrawing effect of pyrrolic-N can activate the adjacent carbon atoms and produce a net positive charge on neighboring carbons. This charge polarization assists the adsorption and reduction of the oxygen molecule on carbon atoms [30]. The result of electrochemical measurements and XPS analysis indicates that pyrrolic-N, rather than pyridinic-N, is the N functionality most responsible for the ORR catalytic activity. Therefore, the pyrrolic-N configurations may be the electrocatalytically active sites.

Table 2
ORR catalytic activity data from Fig. 2(a) for BP1000, BP3501000, and BP350C1000 before and after AAT.

Sample	E_{ORR}/V	E_{hw}/V	j/mA cm^{-2} @ 0.70 V	j/mA cm^{-2} @ 0.40 V
BP1000	0.85	0.64	0.28	1.13
BP3501000	0.87	0.68	0.49	1.16
BP350C1000	0.90	0.78	1.00	1.24
BP350C1000 after AAT	0.88	0.75	0.87	1.19

Although the PB350C1000 electrocatalyst shows excellent electrocatalytic activity for ORR, good long-term stability is also essential for practical application. After the AAT, the losses of E_{onset} and E_{hw} for the ORR of BP350C1000 are 20 and 30 mV, respectively, which demonstrates a higher stability than the Pt/C electrocatalyst [26]. The outstanding stability of the BP350C1000 may be due to the presence of catalytically active sites in the graphitic layers and the strong interactions of the C—N covalent bonds. In addition, the nature of the nitrogen-doped active sites differs from that of Pt-based catalysts [7].

The Tafel method was used to analyze the current–potential (j–E) curves in the kinetic range. The ORR current density is nearly independent of the electrode rotation rate in the potential range of 0.78–0.88 V (vs. RHE), suggesting that the current density in this low-overpotential range is dominated by the electrochemical kinetic current density. The Tafel plots of E as a function of log (j) are shown in Fig. 2(b). A Tafel slope of 84.8 mV decade^{-1} is obtained for BP350C1000, with an electron transfer coefficient (α) of 0.69. The similarity in the Tafel slope values between BP350C1000 and Pt/C is indicative of the same ORR catalysis pathway [26]. The deviation of the Tafel slopes for both BP1000 and BP3501000 from those for BP350C1000 implies that their intermediate adsorption may follow a different model. Higher Tafel slopes (absolute value) correspond to a rapid increase in overpotential with current density, leading to an inferior ORR catalytic activity. The addition of the carbon

support may also play an important role in accelerating charge transfer during ORR.

The ORR mechanism of BP350C1000 was studied further using the RDE at different rotation rates. Koutecky–Levich (K–L) theory is applied to calculate the overall electron transfer numbers (n) based on the fact that the current densities are dependent on the electrode rotation rates in Fig. 2(c). The diffusion-limited current density (j_d) on an RDE was estimated by the K–L equation (Eq. (1)) [31].

$$\frac{1}{j_d} = \frac{1}{j_k} + \frac{1}{0.62nFC_O D_O^{2/3} \nu^{-1/6} \omega^{1/2}} \quad (1)$$

where j_k is the kinetic current density of the ORR; F is the Faradaic constant (96,485 C mol^{-1}); C_O is the O_2 saturation concentration in the aqueous solution (1.2×10^{-6} mol cm^{-3}); D_O is the O_2 diffusion coefficient in 0.1 mol l^{-1} KOH electrolyte (1.9×10^{-5} cm^2 s^{-1}); ν is the kinetic viscosity of the solution (0.01 cm^2 s^{-1}); and ω is the electrode rotation rate (rpm). Fig. 2(d) shows the K–L plot of j_d^{-1} vs. $\omega^{-1/2}$ for BP350C1000.

The linearity and parallelism of the K–L plots indicate consistent electron transfer at different potentials and first-order reaction kinetics with respect to the concentration of dissolved oxygen. The n value for ORR at BP350C1000 was calculated to be $\approx$3.5 from −0.5 to −0.7 V. The ORR catalyzed by BP350C1000 could involve a mixture of two- and four-electron transfer pathways but is dominated by a four-electron transfer pathway to mainly produce H_2O. We also obtained the corresponding kinetic current density of the ORR from 3.5 to 3.66 mA cm^{-2}. These results show that this catalyst would be suitable for catalyzing the ORR in the cathode of fuel cells and metal–air batteries.

4. Conclusions

Herein, we report a facile method to design an ORR electrocatalyst from the pyrolysis of the BP350 pyropolymer combined with a carbon support. The nitrogen exists mainly in the pyridinic- and pyrrolic-N configurations in all carbonized materials. It is interesting that the high-temperature pyrolysis process changes a significant amount of the pyridinic-N to the pyrrolic-N configuration. BP350C1000 contains a higher percentage of the pyrrolic-N configuration, which is promising for four-electron transfer in the ORR. We propose that the pyrrolic-N configuration could function as a catalytically active site for the BP350C1000 prepared in this work. Our study will encourage the production of highly active N-containing catalysts for ORR using native proteins via thermal treatment.

Acknowledgments

This work was supported by the Natural Science Fund of China (Project No. 21273292) and the Fundamental Research Funds for the Central Universities (Project No. CDJXS12220002). We also thank Wenjing Yang and Lin Chen for helpful discussions.

References

[1] F.G. Cheng, J. Chen, Chem. Soc. Rev. 41 (2012) 2172–2192.
[2] N.A. Karim, S.K. Kamarudin, Appl. Energy 103 (2013) 212–220.
[3] Q. Tang, L. Jiang, J. Qi, Q. Jiang, S. Wang, G. Sun, Appl. Catal. B: Environ. 104 (2011) 337–345.
[4] K.P. Gong, F. Du, Z.H. Xia, M. Durstock, L.M. Dai, Science 323 (2009) 760–764.
[5] S.Y. Yang, K.H. Chang, Y.L. Huang, Y.F. Lee, H.W. Tien, S.M. Li, Y.H. Lee, C.H. Liu, C.C.M. Ma, C.C. Hu, Electrochem. Commun. 14 (2012) 39–42.
[6] B. Zheng, J. Wang, F.B. Wang, X.H. Xia, Electrochem. Commun. 28 (2013) 24–26.
[7] Y.M. Yu, J.H. Zhang, C.H. Xiao, J.D. Zhong, X.H. Zhang, J.H. Chen, Fuel Cells 12 (2012) 506–510.
[8] Y.H. Lee, Y.F. Lee, K.H. Chang, C.C. Hu, Electrochem. Commun. 13 (2011) 50–53.
[9] J. Maruyama, I. Abe, Chem. Mater. 18 (2006) 1303–1311.
[10] J. Maruyama, J.J. Okamura, K. Miyazaki, I. Abe, J. Phys. Chem. C 111 (2007) 6597–6600.
[11] Q. Wang, Z.Y. Zhou, D.J. Chen, J.L. Lin, F.S. Ke, G.L. Xu, S.G. Sun, Sci. China Chem. 53 (2011) 2057–2062.
[12] P.B. Xi, Z.X. Liang, S.J. Liao, Int. J. Hydrogen Energy 37 (2012) 4606–4611.
[13] R.Z. Jiang, D.T. Tran, J. McClure, D. Chu, Electrochem. Commun. 19 (2012) 73–76.
[14] J. Maruyama, I. Abe, J. Electrochem. Soc. 154 (2007) B297–B304.
[15] J. Maruyama, N. Fukui, M. Kawaguchi, I. Abe, J. Power Sources 182 (2008) 489–495.
[16] V. Nallathambi, J.W. Lee, S.P. Kumaraguru, G. Wu, B.N. Prov, J. Power Sources 183 (2008) 34–42.
[17] H.B. Li, W.J. Kang, L. Wang, Q.L. Yue, S.L. Xu, H.S. Wang, J.F. Liu, Carbon 54 (2013) 249–257.
[18] Z.Y. Lin, G.H. Waller, Y. Liu, M.L. Liu, C.P. Wang, Nano Energy 2 (2013) 148–241.
[19] C.Z. Guo, C.G. Chen, Z.L. Luo, Int. J. Electrochem. Sci. 8 (2013) 8940–8950.
[20] C.Z. Guo, C.G. Chen, Z.L. Luo, Chin Sci Bull 7 (2013). http://dx.doi.org/10.1007/s11434-013-5995-8.
[21] M. Bystrzejewski, M.H. Rummeli, T. Gemming, H. Lange, A. Huczko, New Carbon Mater. 25 (2010) 1.
[22] S.M. Unni, S. Devulapally, N. Karjule, S. Kurungot, J. Mater. Chem. 22 (2012) 23506–23513.
[23] R. Balgis, G.M. Anilkumar, S. Sago, T. Ogi, K. Okuyama, J. Power Sources 203 (2012) 26–33.
[24] N. Passe-Coutrin, S. Altenor, D. Cossement, C. Jean-Marius, S. Gaspard, Microporous Mesoporous Mater. 111 (2008) 517–522.
[25] C.Y. Liu, B. Xu, Y.W. Tang, G.P. Cao, Y.S. Yang, T.H. Lu, Acta Phys. Chim. Sin. 27 (2011) 604–608.
[26] H. Jin, H.M. Zhang, H.X. Zhong, J.J. Zhang, Energy Environ. Sci. 4 (2011) 3389–3394.
[27] T. Onodera, S. Suzuki, T. Mizukami, H. Kanzaki, J. Power Sources 196 (2011) 7994–7999.
[28] R. Liu, D. Wu, X. Feng, K. Müllen, Angew. Chem. Int. Ed. 49 (2010) 2565–2569.
[29] E. Yoo, J. Nakamura, H. Zhou, Energy Environ. Sci. 5 (2012) 6928–6932.
[30] L. Yu, X. Pan, X. Cao, P. Hu, X. Bao, J. Catal. 282 (2011) 183–190.
[31] A.J. Bard, L. Faulkner, Electrochemical Methods, second ed., Wiley & Sons, New York, 2001.